PHOTOCATALYTIC DEGRADATION OF HUMIC ACID IN WATER BY PVP-DOPED SnO_2/TiO_2 THIN FILM COATED GLASS FIBERS UNDER SOLAR LIGHT IRRADIATION

P. KONGSONG[a*], L. SIKONG[b], M. MASAE[c]
[a]*Department of Materials Engineering, Faculty of Engineering and Architecture, Rajamangala University of Technology Isan, Nakhon Ratchasima 30000, Thailand*
[b]*Department of Mining and Materials Engineering, Faculty of Engineering, Prince of Songkla University, Hat Yai, Songkhla 90112, Thailand*
[c]*Department of Industrial Engineering, Faculty of Engineering, Rajamangala University of Technology Srivijaya, Songkla 90000, Thailand*

The study focuses on the degradation of humic acid (HA) by PVP–doped SnO_2/TiO_2 composite thin films coated on glass fibers were prepared by sol–gel and dip–coating methods. The effects of nitrogen doping on coating morphology, physical properties, and HA degradation rates were experimentally determined. PVP doping results in shifting the absorption wavelengths and narrowing the band gap energy those lead to enhancement of photocatalytic performance. The near optimal $40PVP/SnO_2/TiO^1_2$ composite thin film exhibited about 2 folds of HA degradation rates compared to the TiO_2 films when photocatalytic treatment were performed under solar irradiations due to its narrowest band gap energy (optical absorption wavelength shifting to visible light region) and small crystallite size influenced by PVP doping.

(Received December 19, 2016; Accepted March 17, 2017)

Keywords: PVP doped SnO_2/TiO_2; Sol-gel methods; Glass fibers; Humic acid

1. Introduction

Natural organic matter (NOM) is widely distributed in soil, natural water, and sediments and consisted of a mixture of the decomposition products of plant and animal residues. The main components of NOM are humic acid (HA) and fulvic acid (FA) [1]. HA is responsible for an undesirable colour and has been implicated in bacterial growth in water The presence of HA in natural water can not only damnably affect visual effects and taste, but also increase levels of complexed heavy metals and adsorbed organic pollutants. In addition, HA can react with chlorine during water treatment, thereby producing carcinogenic disinfection by-products (DBPs) [2]. More than 600 compounds of DBPs have been confirmed, such as trihalomethanes, haloacetic acids, which can cause cancer, carcinogenic, mutagenic, and other toxic effects in human being. Hence, removal of HA in water has attracted much of environmental and healthy considerations. Until now, many methods have been adopted to remove HA, including coagulation/flocculation separation, ion exchange, membrane filtration, and adsorption. Photocatalytic degradation as an advanced oxidation processes has recently attracted much attention for the removal of HA. In the photocatalysis reaction, the most frequently used catalyst is TiO_2 [3].

Currently TiO_2 is the most common photocatalyst well suited for water treatment because it is stable in water, non–toxic by ingestion, and low cost [4]. Its photocatalytic mechanism in water and air cleaning is through highly active radical species produced at TiO_2 surface under UV irradiation: hydroxyl radicals are generated by photoholes from the TiO_2 valence band, and superoxide ions are formed due to interaction of photoelectrons from conduction band with molecular oxygen. These participate in a series of oxidation reactions resulting in the destruction of organic contaminants [5].

*Corresponding author : physics_psu@windowslive.com

Recently, there have been great advances in the development of highly efficient TiO_2 films immobilized on support materials. TiO_2 particles in a system have been typically used for water treatment thanks to their high catalytic surface area and significantly much lower, mass transfer limitations. However, the nanosized white TiO_2 particles must be removed before the finished water is reused or discharged to the environment because of aesthetic reasons and most importantly because of possible toxicity of TiO_2 of nanosize dimensions [6]. The techniques to improve photoactivity include control of crystallinity, morphology, crystallite size, and reduction of band gap energy. Doping TiO_2 with N and SnO_2 could increase its photochemical activity [7-8], as metal and metal oxides are known to enhance the activity

In order to enhance the photocatalytic activity of TiO_2 for its practical use and commerce, it is important to decrease the recombination of photogenerated charge carriers. Coupling TiO_2 with other semiconductors can provide a beneficial solution for this drawback. For example, Tada et al. and Vinodgopal et al. [9-10] conducted a systematic research on the SnO_2 as a coupled semiconductor and confirmed that the photogenerated electrons in the SnO_2/TiO_2 system can accumulate on the SnO_2 and photogenerated holes can accumulate on the TiO_2 because of the formation of heterojunction at the SnO_2/TiO_2 interface, which can result in lower recombination rate of photogenerated charge carriers and higher quantum efficiency and better photocatalytic activity [11].

Nitrogen doped titanium dioxide is attracting a continuously increasing attention because of its potential as material for environmental photocatalysis. Many authors have reported that N–doped titanium dioxide. While some authors claim that the band gap of the solid is reduced due to a rigid valence band shift upon doping, others attribute the observed absorption of visible light by $N–TiO_2$ to the excitation of electrons from localized impurity states in the band–gap. Interestingly, it appears that the N–doping induced modifications of the electronic structure may be slightly different for the anatase and rutile polymorphs of TiO_2 [12].

The aim of this work is to assess the degradation of HA contaminant in water by photocatalytic treatments, using N–doped SnO_2/TiO_2 composites and TiO_2 as baseline, coated on glass fibers. An optimum level of nitrogen doping was determined, for maximizing the degradation rate of HA. The films were also characterized for their morphology, anatase crystallinity, and band gap energy and considered fundamental explanatory characteristics affecting photocatalytic activity.

2. Experimental

2.1. Material and Methods

Three coating layers were deposited on glass fibers of type E–glass by the sol–gel process using the dip–coating method. The specific surface area of the starting glass fiber materials is 0.05 m^2g^{-1} and diameter is about 20 μm. The coating sol for the first layer film was a SiO_2/TiO_2, prepared by dissolving 9 ml titanium tetra–isopropoxide (TTIP, 99.95%, Fluka Sigma–Aldrich) and 0.07 ml tetraethylorthosilicate (TEOS, 98%, Fluka Sigma–Aldrich) with 145 ml ethanol, stirring at room temperature with a speed of 800 rpm for 60 min to achieve the mole ratio of $TTIP:C_2H_5OH = 1:82$ then adding 2 M HCl into the sol to adjust pH to be about 3.5. The coating sol for the second and third layers were the N–doped SnO_2/TiO_2 composite, prepared by dissolving certain amounts of TTIP, polyvinylprrrolidone (PVP), and 0.315 g tin (IV) chloride pentahydrate (98%, Riedel DeHaën) with 145 ml ethanol, stirring at room temperature with a speed of 800 rpm for 60 min then adding 2 M HCl into the sol to adjust pH to be about 3.5. The concentration of SiO_2 in TiO_2 of the first layer was fixed at 5mol%, while in the second and third layer 3mol% SnO_2 was used (13). Nitrogen of 0–40 mol% was doped into the SnO_2/TiO_2 composite films following Hao–Li Qin and co–workers [7].

Before coating, the glass fibers were heated at 500°C for 1 h in order to remove wax, cleaned in an ultrasonic bath by using ethanol and dried at 105°C for 24 h. A dip–coating apparatus was used to coat the fibers. Firstly, SiO_2/TiO_2 sol was coated on glass fibers as a compatibilizer layer and followed with PVP–doped SnO_2/TiO_2 sol on top for another two layers. The sol could be homogenously coated on the substrate at the dipping speed of 1.0 mm/s.

Secondly, gel films of TiO_2 composites were obtained by drying at 60°C for 30 min before calcination at 600°C for 2 h at a heating rate of 10°C/min. After that the TiO_2 composite films coated glass fibers were cleaned with distilled water in an ultrasonic bath for 15 min in order to remove the TiO_2 free particles, dried at 105°C for 24 h and kept in a desiccator until use in experiments [13-14].

2.2 Material characterizations

The surface morphology of the prepared films were characterized by scanning electron microscopy (SEM, Quanta, FEI) and atomic force microscopy (AFM) Multi–Mode scanning probes Veeco NanoScope IV with a scan area of 2 × 2 µm. The chemical composition of the films was investigated by X–ray photoelectron spectrometer (XPS; AXIS ULTRA^{DLD}, Kratos analytical, Manchester, UK). Spectrums were process on software "VISION II" by Kratos analytical, Manchester, UK. The base pressure in the XPS analysis chamber was about $5x10^{-9}$ torrs. The samples were excited with X–ray hybrid mode 700x300 µm spot area with a monochromatic Al $K_{\alpha\ 1,2}$ radiation at 1.4 keV. X–ray anode was run at 15kV, 10 mA and 150 W. The photoelectrons were detected with a hemispherical analyzer positioned at an angle of 45^o with respect to the normal to the sample surface. Crystallinity composition was characterized by using an X–ray diffractometer (XRD) (Phillips E'pert MPD, Cu–Kα). The crystallite size was determined from XRD peaks using the Scherer equation [15],

$$D=0.9\lambda/\beta cos\theta_\beta \quad (1)$$

where D is crystallite size, λ is the wavelength of X–ray radiation (Cu–Kα = 0.15406 nm), β is the angle width at half maximum height, and θ_β is the half diffraction angle of the centroid of the peak in degrees. The band gap energies of TiO_2 and TiO_2 composites, in powder form, were measured by UV–Vis–NIR Spectrometer with an integrating sphere attachment (Shimadzu ISR–3100 spectrophotometer), by using $BaSO_4$ as reference.

2.3 Photodegradation of HA

The photocatalytic activities of TiO_2, SnO_2/TiO_2 and PVP–doped SnO_2/TiO_2 thin films coated glass fibers were tested by the degradation of HA solution. The 50 ml HA solution with an initial concentration of 10 ppm was treated with 2 g of TiO_2 film coated glass fibers under solar light irradiation and reaction times up to 6 h were observed. The photocatalytic degradation of HA was also performed under solar light irradiation at Prince of Songkla University, Hat Yai, Songkhla, Thailand (latitude 7.005922 N, longitude 100.502468 E) in October, 2016, between 9 am to 3 pm (0.12 W/cm^2 light intensity), 51-73% relative humidity, and 31–34°C. The remaining concentration of HA was determined by UV–Vis spectrophotometer.

3. Results and discussion

3.1. XRD of TiO_2 thin films

The XRD patterns of TiO_2, along with undoped and PVP–doped SnO_2/TiO_2 thin films, after calcination at 600°C for 2 h, are shown in Fig.1. Comparisons with the JCPDS 21–1272 anatase card of ASTM (American Society for Testing and Materials), and the JCPDS 21–1276 rutile ASTM card, suggest that all samples had anatase phase. The peaks corresponding to different crystallographic planes against an almost flat base line suggest the formation of polycrystalline compounds [16]. The very broad diffraction peaks at (1 0 1) plane (2θ = 25.3°) of PVP–doped SnO_2/TiO_2 thin films were due to small crystallite size of TiO_2. The crystallite sizes calculated from Scherrer's equation are shown in Table 1. It is well known that particle sizes play a vital role in photocatalytic activity since smaller crystals offer greater surface area to volume ratios and thus induce better surface absorbability of hydroxyl/water, which in–turn acts as an active oxidizer in the photocatalytic reaction [17]. The relatively broad peaks of the XRD patterns imply the small crystallite size of anatase [18]. The 30PVP/SnO_2/TiO_2 composite film calcined at 600°C had the smallest 8.4 nm crystallite size apparently decreased by the PVP doping. The

crystallite size decreased with the PVP content increased. Nitrogen seems to hinder phase transformation from amorphous to anatase, as 30PVP/SnO_2/TiO_2 film had the lowest degree of crystallinity, while SnO_2/TiO_2 had the highest degree (Fig.1). It can therefore be concluded that the level of nitrogen doping has a significant effect on the crystallite size of TiO_2 grown during the doping process. It is known that both crystallite size and degree of crystallinity affect photocatalytic activity, so these physical characteristics corroborate the potential of PVP–doping for such effects.

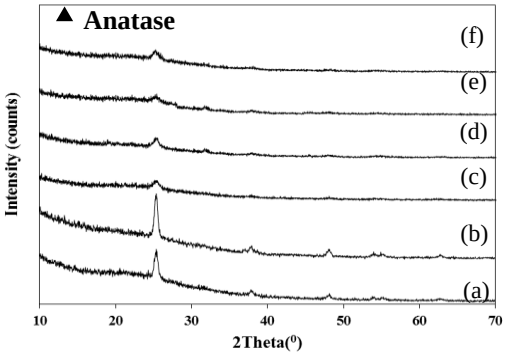

Fig. 1: XRD patterns of thin films calcined at 600°C: (a) TiO_2 (b) SnO_2/TiO_2 (c–f) 10, 20, 30 and 40 mol% PVP/SnO_2/TiO_2, respectively

Table 1: Crystallite sizes and energy band gaps of the calcined thin films synthesized

Samples	Crystallite size (nm)	Energy band gap (eV)
TiO_2	17.2	3.20
SnO_2/TiO_2	17.2	3.20
10PVP/SnO_2/TiO_2	12.9	3.06
20PVP/SnO_2/TiO_2	10.3	3.05
30PVP/SnO_2/TiO_2	8.4	3.01
40PVP/SnO_2/TiO_2	8.6	2.94

3.2 Morphology of thin film surface

The morphology of TiO_2 films coated on glass fibers were observed by SEM as illustrated in Fig. 2. It can be seen that the anatase crystallinity nucleated is homogeneous and has a smooth surface. However, excess TiO_2 seems to be randomly deposited on glass fiber surfaces. Agglomeration of nanoparticles was clearly found for SnO_2/TiO_2 film (Fig.2 (f)) but not for undoped TiO_2 (Fig.2 (d)) and 40PVP/SnO_2/TiO_2 films (Fig.2 (h)). PVP doping hindered the anatase crystal growth and reduced the crystallite size in agreement with the XRD results shown in Fig.1. The morphology of the composite TiO_2 thin film coating surface observed by AFM illustrated in Fig.3. It can be seen that crystals of the anatase phase nucleated from the thin film are homogeneous. The average surface roughness of TiO_2, SnO_2/TiO_2 and 40PVP/SnO_2/TiO_2 thin film found from AFM images are about 9, 11, and 2 nm, respectively. The SnO_2/TiO_2 thin film exhibits more roughness surface compared with 40N/SnO_2/TiO_2 and pure TiO_2 films because of the agglomeration of nanocrystallines. It is noted that the grain sizes of pure TiO_2, SnO_2/TiO_2 and 40PVP/SnO_2/TiO_2 films are estimated by AFM images about 40–50, 50–60 and 20–30 nm, respectively. This smallest grain size affected by nitrogen doping promotes the great photocatalytic activity of the 40PVP/SnO_2/TiO_2 film.

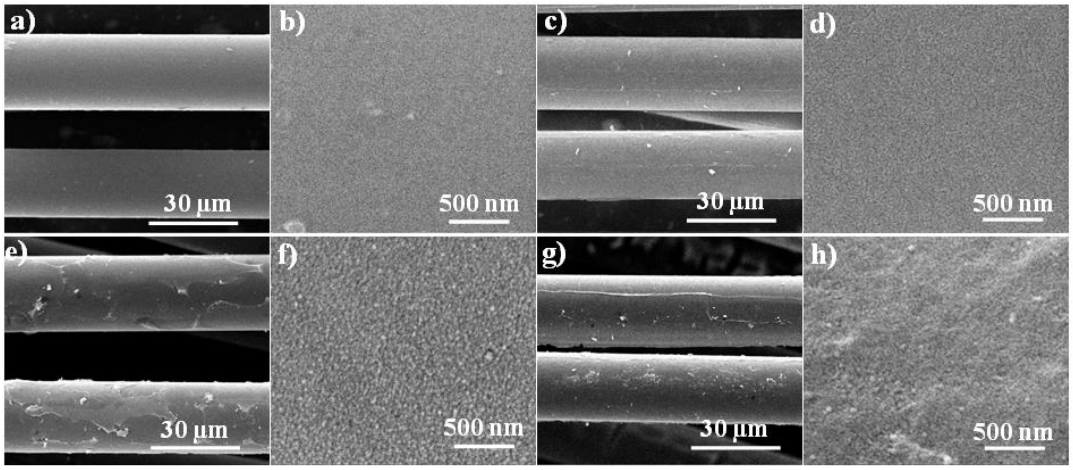

Fig. 2: SEM images of glass fibers, some coated and calcined at 600°C. (a) uncoated 1,500x, (b) uncoated 60,000x, (c) TiO_2 1,500x, (d) TiO_2 60,000x, (e) SnO_2/TiO_2 1,500x, (f) SnO_2/TiO_2 60,000x, (g) 40PVP/SnO_2/TiO_2 1,500x, and (h) 40PVP/SnO_2/TiO_2 60,000x.

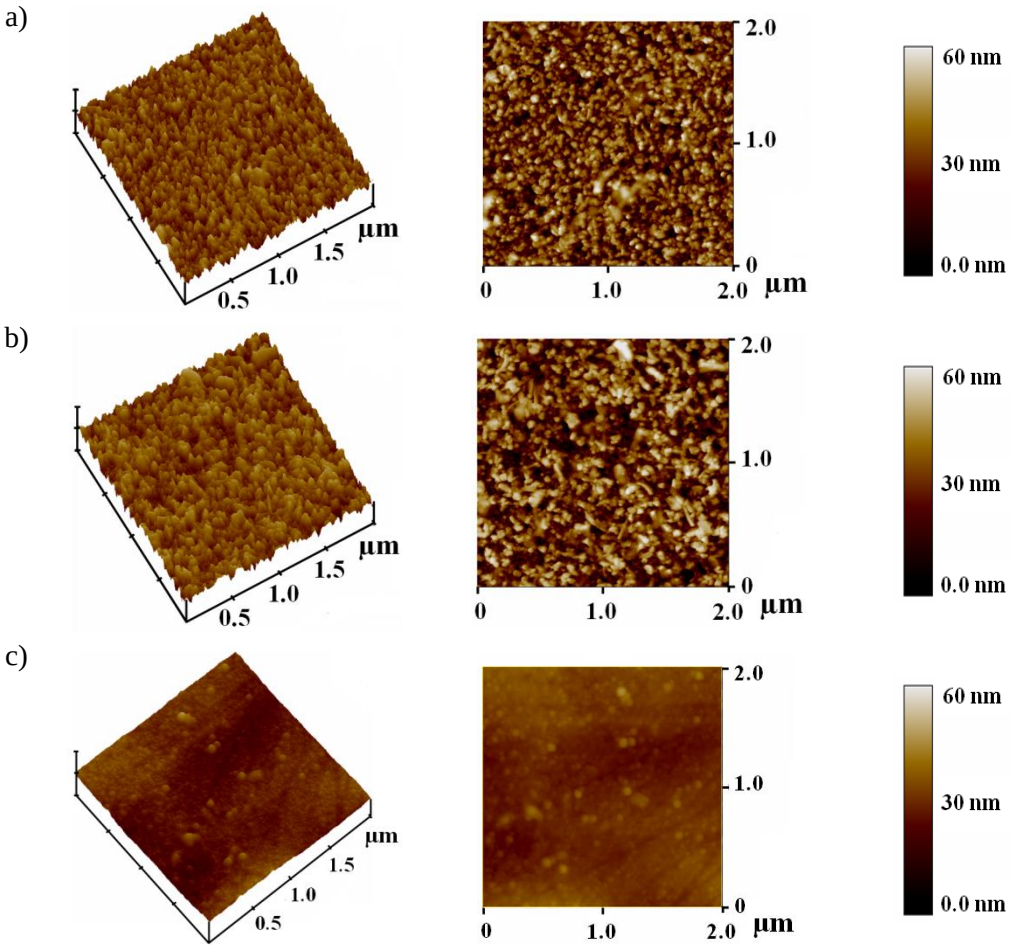

Fig. 3: AFM image with a scan area of 2 × 2 µm of (a) pure TiO_2, (b) SnO_2/TiO_2 and 40PVP/SnO_2/TiO_2 films coated on glass fibers and calcined at 600 ˚C

3.4 Band gap energy determination

The UV–vis spectra of pure TiO_2 and composite TiO_2 are shown in Fig. 4. The absorption edge of the samples was determined by the following equation,

$$E_g = 1239.8/\lambda \quad (2)$$

where E_g is the band gap energy (eV) of the sample and λ (nm) is the wavelength of the onset of the spectrum. The undoped TiO_2 catalyst exhibited absorption only in the UV region with the absorption edge around 400 nm. The band gap energies of the PVP–doped SnO_2/TiO_2 catalysts listed in table 1 were slightly narrower than that of the undoped TiO_2 (3.20 eV). Dopants affect the UV–vis spectra by inhibiting recombination of electron–hole pairs, here especially for the PVP–doped specimens. The band gap energy of PVP–SnO_2/TiO_2 was shifted by 0.14–0.26 eV relative to 3.20 eV for pure TiO_2. The band gap energy of 40N/SnO_2/TiO_2 was 2.94 eV. The band gap energy of TiO_2 tends to decrease with increasing PVP content. These shifts demonstrate how photocatalytic activity may be modulated by atomic–level doping of a nano–catalyst. The absorption wavelength of the 40PVP/SnO_2/TiO_2 photocatalyst is extended towards visible light (λ = 421.7 nm), relative to the other samples [19], giving it the highest photocatalytic activity. The PVP doping slightly decreased the band gap to 2.94 eV by formation of localized N 2p states just above the valence band maximum of TiO_2, due to substitutional N species [20]. When the amount of PVP doping increased, the degree of crystallinity of anatase (TiO_2) decreased, resulting in reduction of crystallite size. In addition, the N interstitial atoms incorporated into the TiO_2 lattice has an effect on the light absorption edge shifting to longer wave length in visible region, leading to the reduction of band gap energy.

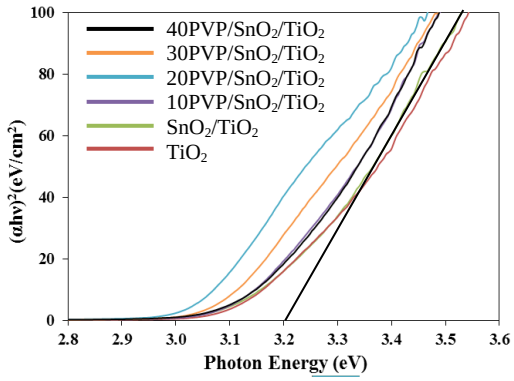

Fig. 4: The photon energy versus $(\alpha h\nu)^2$ curve of representative pure TiO_2 and PVP doped 3SnO_2/TiO_2 samples calcined at 600°C.

3.5 XPS analysis

Fig. 5 shows the X–ray photoelectron spectroscopic (XPS) survey spectra of TiO_2 and 40PVP/SnO_2/TiO_2 thin films. The elements Ti, O, N, and Sn were clearly detected, and the semi–quantitative analysis estimated atomic fractions in this order were about 16.8, 63.7, 0.5, and 0.7 at%, for the 40N/SnO_2/TiO_2 thin film. The XPS peaks indicate that the co–doped TiO_2 thin films contain Ti, Sn, O, and N elements, and the binding energies of Ti 2p, Sn 3d, O 1s, and N 1s are 458, 496, 525, and 400 eV, respectively. The Sn 3d XPS peaks of Sn–TiO_{2-x}, shown in Fig.6a), demonstrate existence of stannous species on the surface of TiO_2. The Sn $3d_{5/2}$–binding energy of Sn–TiO_{2-x} at 486.1 eV was below the 486.6 eV reference value found in literature [21]. To assess the state of nitrogen atoms in the 40PVP/SnO_2/TiO_2 thin films, high–resolution XPS spectra of N 1s region were generated, as shown in Fig.6b). The peak at 400.1 eV could be attributed to the interstitial nitrogen atoms in crystal lattice of TiO_2 as Ti–O–N structural feature [22]. This form Ti-O-N linkages, reducing the band gap energy beneficially for the photocatalytic properties of 40PVP/SnO_2/TiO_2 films.

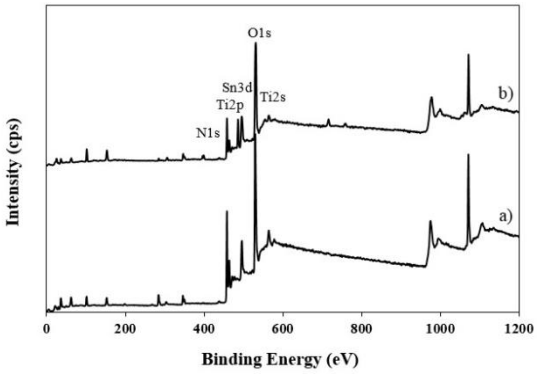

Fig. 5 XPS spectra of a) TiO_2 and b) 40N/SnO_2/TiO_2 thin films samples calcined at 600°C.

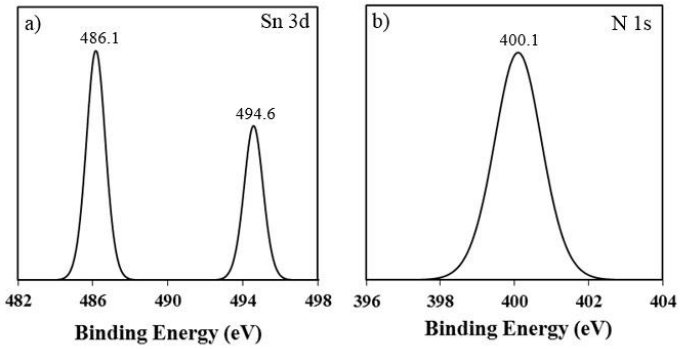

Fig. 6: XPS spectrum of a) Sn 3d and b) N 1s on the surface of 40PVP/SnO_2/TiO_2 thin films samples calcined at 600°C.

3.6 Photocatalytic degradation of HA

The photocatalytic activities of the films on glass fibers were determined for degradation of HA, with an initial concentration of 10 ppm, under solar light for various irradiation times. The apparent degradation rate constant (k) was chosen as the basic kinetic parameter to compare the photocatalysts. The observed C_0/C vs. irradiation time is plotted in Fig. 7. The fitted k values are shown in Table 3. Where C is the concentration of HA remaining in the solution at irradiation time t, and C_0 is the initial concentration at t = 0. The rate constant k is enhanced by PVP doping, and the 0.341 h^{-1} rate constant for the 40PVP/SnO_2/TiO_2 film is about 2 folds relative to pure TiO_2 under solar light irradiation (Fig. 7). The 40N/SnO_2/TiO_2 thin film has optimal photocatalytic activity across the range of compositions tested. According to prior reports, various factors affect the photoactivity of TiO_2 photocatalysts, including crystallinity, grain size, specific surface area, surface morphology and surface state (surface OH radicals), and these factors are not independent but closely related to each other [23-24]. Doping TiO_2 with a suitable amount of nitrogen (40 mol%) in SnO_2/TiO_2 composite films shifted light absorption wavelength to the visible region, reduced crystallite size to be about 8.6 nm, and narrowed the energy band gap to 2.94 eV (Table 1) [25]. The undoped TiO_2 samples have little ability to degrade the contaminant while the SnO_2/TiO_2 samples modified with nitrogen display higher activity owing to the spectral response in visible light region. Compared to the undoped TiO_2, the PVP doped SnO_2/TiO_2 films had a significantly higher degradation, from the spectral response in the visible light region. This is due to the PVP doping into the TiO_2 lattice to form an intermediate energy level, and leading to the narrow band gap of PVP–doped SnO_2/TiO_2 films. Well–crystallized anatase facilitates the transfer of photo–induced vacancies from bulk to surface, for the degradation of organic composites, and effectively inhibits the recombination between photo generated electrons and holes. As seen in Fig.1, the 30N/SnO_2/TiO_2 thin film had the smallest crystallite size estimated. It is believed that

the photocatalytic degradation reaction of organic pollutants occurs on the surface of TiO_2, and O_2 and H_2O are necessary for the photocatalytic degradation. Under UV irradiation, electron–hole pairs are created on the TiO_2 surface. Oxygen adsorbed on the TiO_2 surface prevents the recombination of electron–hole pairs by trapping electrons of SnO_2 incorporated in TiO_2; Superoxide radical ions ($^{\cdot}O^{-2}$) are thus formed. $^{\cdot}OH$ radicals are formed from holes reacting with either H_2O or $OH^{\cdot}$ adsorbed on the TiO_2 surface. The main reactions can be described as follows:

$$TiO_2 + h\nu \rightarrow TiO_2 + e^- + h^- \quad (4)$$

$$O_2 + e^- \rightarrow {}^{\cdot}O^{-2} \quad (5)$$

$$H_2O + h^+ \rightarrow {}^{\cdot}OH + H^+ \quad (6)$$

$$OH^- + h^+ \rightarrow {}^{\cdot}OH \quad (7)$$

Correspondingly, H_2O_2 is formed by $^{\cdot}O^{-2}$.

$$^{\cdot}O^{-2} + H+ \rightarrow HO^{\cdot}{}_2 \quad (8)$$

$$HO^{\cdot}{}_2 + HO^{\cdot}{}_2 \rightarrow H_2O_2 + O_2 \quad (9)$$

$$^{\cdot}O + HO^{\cdot}{}_2 \rightarrow HO^-{}_2 + O_2 \quad (10)$$

$$HO^-{}_2 + H^+ \rightarrow H_2O_2 \quad (11)$$

$^{\cdot}OH$ and O_2^{2-} are also formed by H_2O_2

$$H_2O_2 + e^- \rightarrow {}^{\cdot}OH + OH^- \quad (12)$$

$$H_2O_2 + {}^{\cdot}O_2 \rightarrow {}^{\cdot}OH + OH^- + O_2 \quad (13)$$

$$H_2O_2 + h\nu \rightarrow 2{}^{\cdot}OH \quad (14)$$

$$H_2O_2 \rightarrow O_2^{2-} + 2H^+ \quad (15)$$

The $^{\cdot}OH$ and O_2^{2-} are widely accepted as primary oxidants in heterogeneous photocatalysis [26]. The HA molecules then could be degraded into CO_2, H_2O, and other mineralization by the hydroxyl radicals [27].

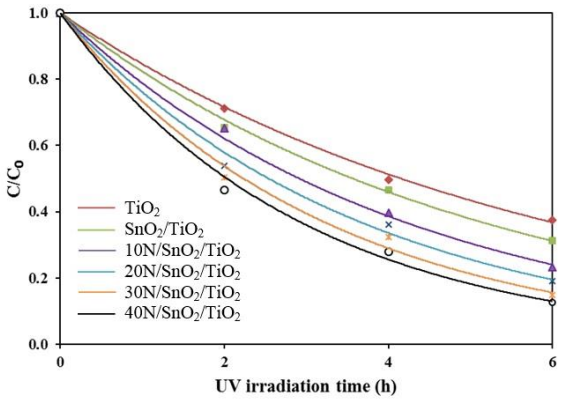

Fig. 7: Photocatalytic degradation kinetics of HA under solar light irradiation. Reaction conditions: C_0 = 10 ppm, catalyst loading: 2 g, reaction time: 6 h

Table 3: The identified kinetics of photocatalytic degradation of HA under solar light irradiation.

Samples	Rate Equation	Rate constant (k), h^{-1}	R^2
TiO_2	$C = e^{-0.167t}$	0.167±0.001	0.997
SnO_2/TiO_2	$C = e^{-0.194t}$	0.194±0.002	0.998
$10N/SnO_2/TiO_2$	$C = e^{-0.238t}$	0.238±0.004	0.997
$20N/SnO_2/TiO_2$	$C = e^{-0.273t}$	0.273±0.004	0.992
$30N/SnO_2/TiO_2$	$C = e^{-0.310t}$	0.310±0.006	0.990
$40N/SnO_2/TiO_2$	$C = e^{-0.341t}$	0.341±0.005	0.994

4. Conclusions

PVP–doped SnO_2/TiO_2 composite films were successfully synthesized and deposited on glass fibers, via sol–gel and dip–coating methods. The coated fibers were calcined at 600°C for 2 h at a heating rate of 10°C/min in order to form crystalline anatase. PVP doping of SnO_2/TiO_2 composite films affected surface smoothness, crystallite size, and band gap energy of the films. The crystallite size and band gap energy of TiO_2 decreased with the increasing PVP content. The $40PVP/SnO_2/TiO_2$ composite film is near optimal across the compositions tested, having narrow band gap energy and small crystallite size, and the highest photocatalytic activity on degradation of HA. The $40PVP/SnO_2/TiO_2$ thin film composite has about 2 times the degradation rate relative to TiO_2 under solar light irradiation. The results suggest that $40PVP/SnO_2/TiO_2$ composite thin film is more effective for treating HA contaminated water under sunlight irradiation.

Acknowledgments

The authors gratefully acknowledge support by the Department of Materials Engineering, Faculty of Engineering and Architecture, Rajamangala University of Technology Isan.

References

[1] J. Fu, M. Ji, Z. Wang, L. Jin, D. An, J. Hazard. Mater. **131**(1-3), 238 (2006).
[2] W.W. Tang, G. M. Zeng, J.L. Gong, J. Liang, P. Xu, C. Zhang, B.B. Huang, Sci. Total Environ. **468–469**, 1014 (2014).
[3] Q. Zhou, Y.H. Zhong, X. Chen, J.H. Liu, X.J. Huang, Y.C. Wu, J. Mater. Sci. **49**, 1066 (2014).
[4] Q. Li, S. Mahendra, D.Y. Lyon, L. Brunet, M.V. Liga, D. Li, P.J. Alvarez, Water Res. **42**(18), 4591 (2008).
[5] E.V. Skorb, L.I. Antonouskaya, N.A. Belyasova, D.G. Shchukin, H. Möhwald, D.V. Sviridov, Appl. Catal. B Environ. **84**(1-2), 94 (2008).
[6] M. Diallo, J. Duncan, N. Savage, A. Street R. Sustich, Nanotechnology Applications for Clean Water, NY, USA, (2009).
[7] H.L. Qin, G.B. Gu, S. Liu, Chimie. **11**(1-2), 95 (2008).
[8] L.C. Chen., F.R. Tsai, S.H. Fang, Y.C. Ho, Electrochim. Acta. **54**(4), (2009).
[9] H. Tada, Y. Konishi, A. Kokubu, S. Ito, Langmuir **20**, (2004).
[10] K. Vinodgopal, P.V. Kamat, Environ. Sci. Technol. **29**, 841 (1995).
[11] M. Zhou, J. Yu, S. Liu , P. Zhai, L. Jiang, J. Hazard. Mater. **154**(1-3) 1141 (2008).
[12] C.D. Valentin, E. Finazzi, G. Pacchioni, A. Sellonib, S. Livraghi, M.C. Paganini, E. Giamello, Chem. Phys. **339**(1-3), 44 (2007).
[13] P. Kongsong, L. Sikong, S. Niyomwas, V. Rachpech, Sci. World J. **2014**, 1 (2014).
[14] P. Kongsong, L. Sikong, S. Niyomwas, V. Rachpech, Photochem. Photobiol. **90**, 1243(2014).

[15] Z. Liuxue, L. Peng, S. Zhixing, Chem. Phys. **98**, 111 (2006).
[16] M. Thomas, S.K. Ghosh, K.C. George, Mater. lett. **56**(4), 386 (2002).
[17] G. Yang, Z. Jiang, H. Shi, T. Xiao, Z. Yan, J. Mater. Chem. **20**, 5301 (2010).
[18] D. Wang, L. Xiao, Q. Lau, X. Li, J. An, Y. Duan, J. Hazard. Mater. **192**, 150 (2011).
[19] L. Sikong, M. Masae, K. Kooptarnond, W. Taweepreda F. Saito, App. Surf. Sci. **258**(10), 4436 (2012).
[20] R. Jaiswal, N. Patel, D.C. Kothari, A. Miotello, Appl. Catal. B. Environ. **126**, 47 (2012).
[21] B. Xin., D. Ding, Y. Gao, X. Jin, H. F, P. Wang, App. Surf. Sci. **255**(11), 5896 (2009).
[22] H. Wang, X. Gao, G. Duan, X. Yang, X. Liu, J. Environ. Chem. Eng. **3**(2), 603 (2015).
[23] A. Zaleska, W. Sobezak, E. Grabowska, J. Hupka, Appl. Catal. B. Environ. **78**(1-2), 92 (2008)
[24] X. Zhang, Q. Liu, Mater. Lett. **62**(17-18), 2589 (2008).
[25] J. Ying, H. Bai, Q. Jiang, J. Lian, Thin Solid Films **516**(8), 1736 (2008).
[26] C. Shifu, L. Yunzhang, Chemosphere. **67**(5), 1010 (2007).
[27] P. Kongsong, L. Sikong, S. Niyomwas, V. Rachpech, Key Engineering Materials **608**, 164 (2014).